

---

The following preprint has been submitted to *Analytical Chemistry*, and has not yet undergone peer-review:  
Hare, V.J. et al., *High-Precision Triple Oxygen Isotope Analysis of Carbon Dioxide by Tunable Infrared Laser Absorption Spectroscopy*.

Subsequent versions of this manuscript may have slightly different content. If accepted, the final version of this manuscript will be available via the 'Peer-reviewed publication DOI' link on the right hand side of this webpage. Please feel free to contact any of the authors; we welcome feedback.

---

July 12, 2022

# High-Precision Triple Oxygen Isotope Analysis of Carbon Dioxide by Tunable Infrared Laser Absorption Spectroscopy

Vincent J. Hare,<sup>\*,†,¶</sup> Christoph Dyroff,<sup>‡</sup> David D. Nelson,<sup>‡</sup> and Drake A. Yarian<sup>†</sup>

<sup>†</sup>*Stable Light Isotope Laboratory, Department of Archaeology, University of Cape Town,  
South Africa*

<sup>‡</sup>*Aerodyne Research Inc., Billerica, Massachusetts 01821, United States*

<sup>¶</sup>*ORCID: 0000-0002-4475-4109*

E-mail: vincent.hare@uct.ac.za

Phone: +27 (0)82 3333778

## Abstract

Precision measurements of the stable isotope ratios of oxygen ( $^{18}\text{O}/^{16}\text{O}$ ,  $^{17}\text{O}/^{16}\text{O}$ ) in  $\text{CO}_2$  are critical to atmospheric monitoring and terrestrial climate research. High-precision  $^{17}\text{O}$  measurements by isotope ratio mass spectrometry (IRMS) are challenging because they require complicated sample preparation procedures, long measurement times, and relatively large samples sizes. Recently, tunable infrared laser direct absorption spectroscopy (TILDAS) has shown significant potential as an alternative technique for triple oxygen isotope analysis of  $\text{CO}_2$ , although the ultimate level of reproducibility is unknown, partly because it is unclear how to relate TILDAS measurements to an internationally-accepted isotope abundance scale (e.g. VSMOW2-SLAP2). Here, we present a method for high-precision triple oxygen isotope analysis of  $\text{CO}_2$  by TILDAS, requiring  $\sim 8\text{-}9\ \mu\text{mol}$  of  $\text{CO}_2$  (or 0.9 mg carbonate) in 50 minutes, plus  $\sim 1.5$  hours for

13 sample preparation and dilution of CO<sub>2</sub> in N<sub>2</sub> to a nominal 400 μmol mol<sup>-1</sup>. Overall  
14 reproducibility of Δ<sup>17</sup>O (CO<sub>2</sub>) was 0.004 ‰ (4 per meg) for IAEA603 (SE, *n* = 6), and  
15 10 per meg for NBS18 (SE, *n* = 4). Values corrected to the VSMOW2-SLAP2 scale  
16 are in good agreement with established techniques of high-precision IRMS, with the  
17 exception of Δ<sup>17</sup>O measured by platinum-catalyzed exchange of CO<sub>2</sub> with O<sub>2</sub>. Com-  
18 pared to high-precision IRMS, TILDAS offers the advantage of ~ 10 times less sample,  
19 and greater throughput, without loss of reproducibility. The flexibility of the technique  
20 should allow for many important applications to global biogeochemical monitoring, and  
21 investigation of <sup>17</sup>O anomalies in a range of geological materials.

22 The most commonly measured isotopologues of CO<sub>2</sub> are <sup>12</sup>C<sup>16</sup>O<sup>16</sup>O, <sup>13</sup>C<sup>16</sup>O<sup>16</sup>O, and  
23 <sup>12</sup>C<sup>16</sup>O<sup>18</sup>O. Paleoenvironmental proxies based on these isotopologues (i.e. δ<sup>13</sup>C and δ<sup>18</sup>O)  
24 are widely used to reconstruct past climates, as well as to quantify the sources and sinks  
25 of CO<sub>2</sub>, which are essential to understanding the global carbon budget. However, on their  
26 own these proxies are often insufficient, and additional constraints are needed to resolve  
27 carbon fluxes, past and present. Photochemical reactions during the formation of ozone are  
28 associated with mass-independent isotope effects which lead to anomalous enrichment in <sup>17</sup>O  
29 in stratospheric CO<sub>2</sub>.<sup>1-4</sup> The <sup>17</sup>O enrichment is passed to the troposphere, and reset close  
30 to zero by mass-dependent isotopic exchange between CO<sub>2</sub> and the terrestrial biosphere  
31 (mostly leaves) and oceans.<sup>5</sup> In terrestrial materials that contain oxygen, as well as the  
32 troposphere, the <sup>17</sup>O anomaly (expressed as Δ<sup>17</sup>O)<sup>6</sup> is a promising tracer for carbon exchange  
33 between reservoirs,<sup>2,5,7</sup> as well as an exciting new proxy for paleoenvironmental change.<sup>8-11</sup>  
34 For the investigation of these effects, high-precision measurement (~0.01‰, or 10 per meg)  
35 of Δ<sup>17</sup>O is required, which is a challenging task for IRMS methods. These methods require  
36 the transformation of CO<sub>2</sub> to O<sub>2</sub> analyte, thereby avoiding isobaric interference between  
37 the <sup>13</sup>C<sup>16</sup>O<sup>16</sup>O and <sup>12</sup>C<sup>17</sup>O<sup>16</sup>O isotopologues, both of nominal mass 45. For this, various  
38 complicated techniques have been developed, including: conversion of CO<sub>2</sub> to O<sub>2</sub>;<sup>9,12</sup> isotopic  
39 exchange of subequal quantities of CO<sub>2</sub> and O<sub>2</sub> over a hot platinum catalyst,<sup>13-15</sup> or by careful

40 equilibration of CO<sub>2</sub> with H<sub>2</sub>O, and subsequent water fluorination to produce O<sub>2</sub>.<sup>16</sup>

41 Recent advances in optical detection of rare isotopologues have led to a rapidly expand-  
42 ing array of applications to biogeochemistry, e.g. detection of radiocarbon dioxide at sen-  
43 sitivities approaching that of accelerator mass spectrometry;<sup>17</sup> high-precision measurement  
44 of multiply-substituted isotopologues of both CH<sub>4</sub>,<sup>18</sup> and CO<sub>2</sub>.<sup>19</sup> The latter techniques all  
45 utilise tunable infrared laser direct absorption spectroscopy (TILDAS) for the direct mea-  
46 surement of isotopologue abundance ratios. Promisingly, Sakai *et al.*<sup>20,21</sup> report TILDAS  
47 measurements of <sup>18</sup>O/<sup>16</sup>O, <sup>17</sup>O/<sup>16</sup>O from small quantities of CO<sub>2</sub> (2-68 μmol), with a preci-  
48 sion of up to 30 per meg (SE,  $n = 10$ ). The advantage of these methods over IRMS is that  
49 they require simpler laboratory procedures, and offer the potential of smaller samples sizes,  
50 and greater throughput. However, their overall reproducibility remains uncertain, and it is  
51 unclear how to relate TILDAS <sup>18</sup>O/<sup>16</sup>O and <sup>17</sup>O/<sup>16</sup>O ratios to commonly-used abundance  
52 scales, such as VSMOW2-SLAP2 or VPDB.

53 Here, we present a relatively simple method for triple oxygen isotope analysis by TILDAS  
54 which uses CO<sub>2</sub> evolved by acid digestion of interlaboratory carbonate reference standards,  
55 as well as a working reference gas, to produce high-precision Δ<sup>17</sup>O analyses, alongside δ<sup>13</sup>C.  
56 We have integrated TILDAS with an automated sample preparation system, which can  
57 also accept CO<sub>2</sub> from break-seal vials, acid digestion of ~ 0.9 mg of carbonate samples, or  
58 dry air from atmospheric flasks. The system ensures that CO<sub>2</sub> is well-mixed in N<sub>2</sub> prior  
59 to measurement, eliminating the possibility of isotope fractionation due to diffusion. We  
60 also present a framework for correcting spectroscopic <sup>18</sup>O/<sup>16</sup>O and <sup>17</sup>O/<sup>16</sup>O ratios to the  
61 VSMOW2-SLAP2 scale, and show that overall reproducibilities from TILDAS can match  
62 those of IRMS methods.

## 63 Experimental Section

### 64 Tunable Infrared Laser Direct Absorption Spectroscopy.

65 Our instrument is a commercial Aerodyne Research Inc. (ARI) tunable infrared laser direct  
66 absorption spectrometer (TILDAS).<sup>19,20,22</sup> The instrument is based on the ARI dual-laser  
67 monitor platform, but is customized to the requirements of measuring CO<sub>2</sub> from carbonates,  
68 diluted to  $\sim 400 \mu\text{mol mol}^{-1}$  in N<sub>2</sub>. In the configuration presented here, the instrument  
69 enables the measurement of multiple isotopologues of CO<sub>2</sub> simultaneously. The instrument  
70 was equipped with two co-aligned distributed-feedback interband-cascade lasers (DFB-ICL,  
71 nanoplus Nanosystems and Technology GmbH). The <sup>12</sup>C<sup>16</sup>O<sup>16</sup>O, <sup>12</sup>C<sup>18</sup>O<sup>16</sup>O, and <sup>13</sup>C<sup>16</sup>O<sup>16</sup>O  
72 isotopologues were targeted in the region of 2310 cm<sup>-1</sup>, and the <sup>12</sup>C<sup>17</sup>O<sup>16</sup>O isotopologue  
73 was targeted in the region of 2349 cm<sup>-1</sup>. The wavelengths of the two lasers were chosen to  
74 achieve both strong and well-balanced absorption signals of the individual isotopologues of  
75 interest at the expected sample-isotopologue ratios.

76 The lasers and data acquisition were controlled by the ARI software TDLWintel, which  
77 also controlled the valve switching system (valves P9-P15 in Fig. 1), which is identical to the  
78 system reported elsewhere.<sup>19</sup> Both lasers were scanned sequentially at a frequency of 1.5 kHz.  
79 Before analysis, 1500 spectra were averaged to achieve a 1-second average spectrum. This  
80 improved the signal-to-noise ratio by approximately  $\sqrt{1500} = 38\times$ . The averaged spectra  
81 were then individually fit to one spectroscopic model per laser. These models include: the  
82 relevant absorption lines of all isotopologues present in each spectral window; a baseline  
83 of a polynomial form; as well as the zero-light signal. The zero-light signal is equivalent to  
84 complete absorption, and the baseline is equivalent to no absorption (complete transmission).

85 Absorption signal enhancement was achieved by increasing the optical absorption path-  
86 length to 36 m using a multipass absorption cell. In this cell, the laser beams were reflected  
87 between two mirrors such that they accumulated 194 passes. Upon exiting the cell, the co-  
88 aligned beams were focused on a thermoelectrically cooled HgCdTe detector (J19, Teledyne

89 Judson). The sample pressure was around 28 Torr (10:1 reduction when expanding from  
90 volume 1, V1, in the valve switching system, previously filled via critical orifice through  
91 solenoid valves E1 (for sample gas) or E2 (for reference gas) see Fig. 1). The reduced pres-  
92 sure was used to sharpen the absorption lines and provide excellent isotopologue selectivity.  
93 This combined with the 36 m path length provided sufficient signal for very-high precision  
94 measurements.

### 95 **Automated CO<sub>2</sub> Preparation System.**

96 The automated CO<sub>2</sub> sample preparation system is designed to cryogenically purify, dilute,  
97 and mix sample CO<sub>2</sub> with N<sub>2</sub>. Samples are able to be introduced to the system by any  
98 of 3 methods: loaded in break-seal tubes, from acid digestion of carbonates (via a Thermo  
99 GasBench II), or directly from a removable atmospheric sampling flask. Each sample intro-  
100 duction pathway is handled with a unique preparation sequence based in a custom LabVIEW  
101 program. The system consists of a break-seal manifold, liquid N<sub>2</sub> cryogenic trap, 3 mixing  
102 volumes (MV1, MV2, MV3 - combined volume 687 mL), and a circulation loop with inline  
103 diaphragm pump (CTS Series, Parker Hannifin Corp., USA) (Fig. 1). Valves 1-7, 16-21  
104 are Swagelok SS4-BK-VA-1C bellows-sealed valves. V8 is a three-way solenoid valve (P/N  
105 009-0294-900, Parker Hannifin Corp., USA). Non-numerically identified valves are manu-  
106 ally toggled. Pressure gauges and corresponding data are handled by a data acquisition  
107 unit (cDAQ-9171, National Instruments Corp., USA). The sampling flask, which doubles as  
108 MV1, is custom made (GlassChem CC, South Africa, 576 mL) and designed to maximize  
109 turbulent mixing, see Supporting Information for photographs.

110 Samples are introduced from their respective source and first cryogenically trapped in  
111 MV2. After a short pump-over to promote purification and complete sample collection, CO<sub>2</sub>  
112 is thawed for 6 minutes and the yield measured (Agilent Varian CDG-500, 0-10 Torr). Sample  
113 yield is then used to calculate dilution and mixing requirements on a sample specific basis  
114 (target dilution is 400  $\mu\text{mol mol}^{-1}$ ) before being expanded into MV1. Ultra high-purity N<sub>2</sub>

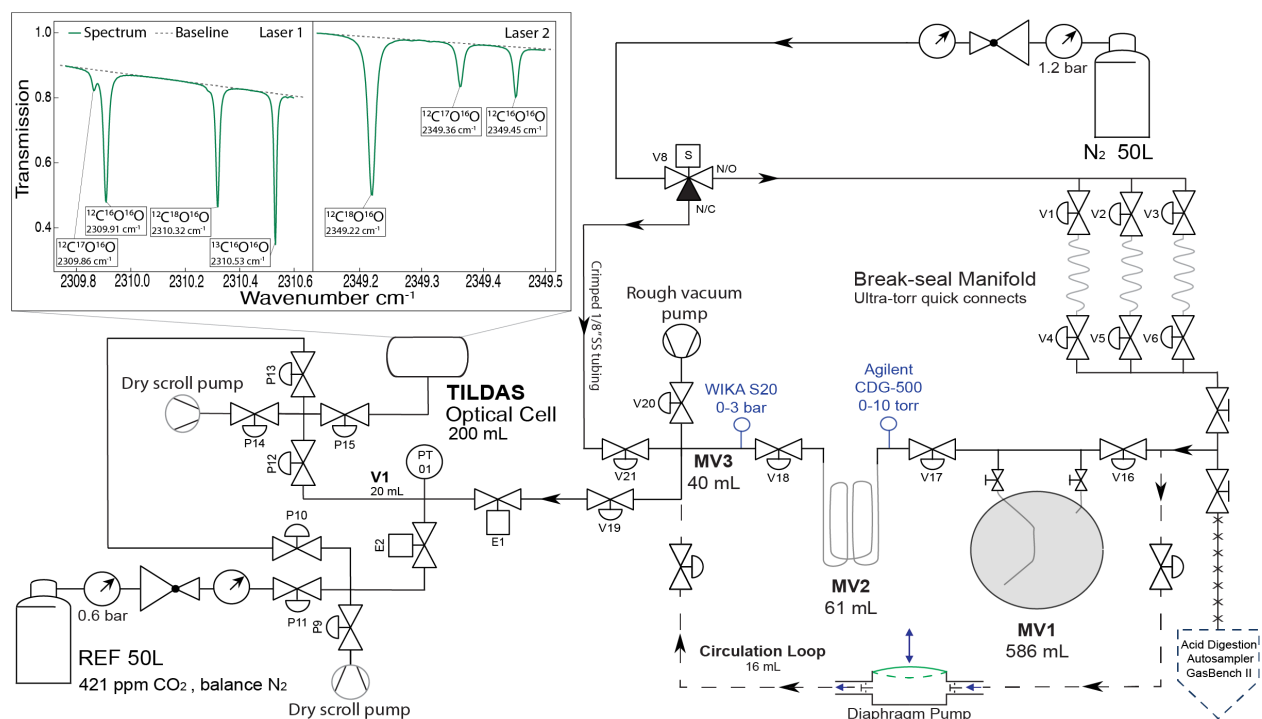


Figure 1: Schematic diagram of the system for automated preparation of CO<sub>2</sub> for high-precision TILDAS measurements of triple oxygen isotopes. MV1, MV2, and MV3 refer to mixing volumes 1 (586 mL), 2 (61 mL), and 3 (40mL). CO<sub>2</sub> from either acid digestion of carbonates (GasBench II) or alternatively, crackers, is frozen into MV2, and then diluted to  $\sim 400 \mu\text{mol mol}^{-1}$  in N<sub>2</sub> in a specially-designed flask (MV1). The entire mixing volume (MV1,2,3) is then circulated for 2.5 minutes to ensure complete mixing prior to measurement. TILDAS sampling valves (pneumatic valves P9-P15, electronic valves E1 and E2) are the same as a previous system.<sup>19</sup> Sampling valves allow for repeated comparisons between a 50L reference tank ( $421 \mu\text{mol mol}^{-1}$  CO<sub>2</sub>), and well-mixed sample in volume MV1,2,3.

115 as the diluent is regulated into the system at 1.2 bar and directed through a critical orifice,  
 116 three-way solenoid valve, and crimped 1/8" stainless steel tubing into MV3 via valve V21.  
 117 Dilution and initial mixing occur simultaneously as MV3 and MV2 are repeatedly pressurized  
 118 with N<sub>2</sub> to 1450 mbar (WIKA S-20, 0-3 bar) and turbulently expanded into MV1. The exact  
 119 number of repeated expansions is unique to each sample as calculated from the sample yield.  
 120 See Supporting Information for detailed sequence summaries and mixing steps.

121 After dilution and initial mixing, samples are further mixed by opening the circulation  
 122 loop and activating the diaphragm pump. Pump circulation is  $750 \text{ mL min}^{-1}$ , meaning that  
 123 three complete circulations occur through MV1,2,3 in 2.5 minutes. After 2.5 minutes the

124 circulation loop closes and sample preparation is complete. Sample gas is then introduced to  
125 the TILDAS valve switching system via valve V19, a critical orifice, and valve E1. Sample  
126 pressures in the combined mixing volume typically begin around  $\sim 750$  mbar and decrease to  
127  $\sim 450$  mbar over the course of an analysis. Overall repeatability of the sample concentration  
128 (evaluated from the  $^{12}\text{C}^{16}\text{O}^{16}\text{O}$  isotopologue) was  $403.6 \pm 8.2 \mu\text{mol mol}^{-1}$  ( $1\sigma$ ,  $n = 17$ ).  
129 Within sample (aliquot) concentration repeatability ranged from 0.4 to 0.9  $\mu\text{mol mol}^{-1}$  ( $1\sigma$ ).  
130 Of importance to the success of our system are the high-precision Agilent Varian CDG-500  
131 pressure gauge, sampling flask design, and circulation loop.

### 132 **Reference Gas and Spectroscopic Measurement Procedure.**

133 The reference used is a custom-made 50L high pressure cylinder of 421  $\mu\text{mol mol}^{-1}$   $\text{CO}_2$  in  
134 ultra high-purity  $\text{N}_2$  (99.999%), made by Air Liquide South Africa (Pty) Ltd in July of 2021.  
135 The reference gas tank was allowed to sit for several months before initial measurements were  
136 made. Reference gas is regulated into the TILDAS at 0.6 bar using a sub-ambient high-purity  
137 absolute pressure regulator (3396 series, Matheson Tri-gas Inc., USA). Aliquots of reference  
138 gas are introduced via valve P11 (Fig. 1), a critical orifice, and valve E2 to an intermediate  
139 volume (V1, 20mL) all of which are part of the TILDAS sampling valve system, described  
140 elsewhere.<sup>19</sup> Sub-ambient regulation of the reference gas is of critical importance as slowing  
141 the fill rate of V1 allows for greater accuracy in achieving the target fill pressure of 300  
142 Torr, and therefore greater repeatability in optical cell pressure throughout an analysis. 0.6  
143 bar is also comparable to sample filling pressures, promoting similar V1 filling accuracy  
144 between gases. Overall aliquot repeatability of the working reference gas concentration for  
145 the  $^{12}\text{C}^{16}\text{O}^{16}\text{O}$  isotopologue was  $421.4 \pm 0.4 \mu\text{mol mol}^{-1}$ , evaluated over 12 hours of repeated  
146 measurement ( $1\sigma$ ,  $n = 148$ ).

147 All aspects of the TILDAS measurement system, (e.g. timings, laser control, data acquisi-  
148 tion, signal processing, etc.) are controlled by dedicated software (TDLWintel). Analyses are  
149 performed by repeatedly alternating aliquots of sample and reference gas into the TILDAS,



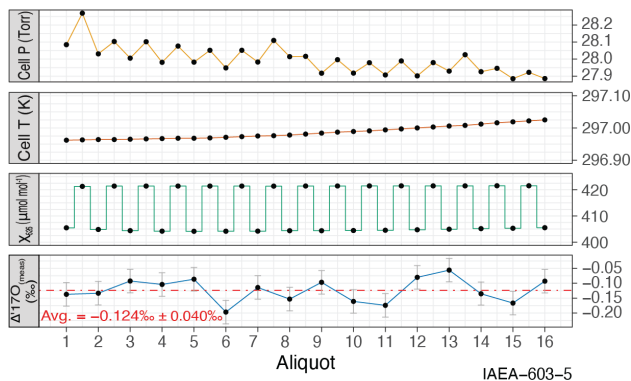


Figure 2: TILDAS measurement procedure. Repeated comparisons between a 50L reference tank ( $421 \mu\text{mol mol}^{-1} \text{CO}_2$ ), and well-mixed sample of  $8.645 \mu\text{mol CO}_2$ , evolved from 0.914 mg of IAEA603 carbonate, by phosphoric acid digestion ( $70^\circ\text{C}$  for 2 hours) and mixed to  $404.8 \mu\text{mol mol}^{-1}$  in  $\text{N}_2$  (703.53 mbar total sample). The measurement sequence takes around 50 minutes. Optical cell temperatures and pressures during this time were stable to within  $<0.1 \text{ K}$  and  $<300 \text{ mTorr}$ , respectively. Laboratory temperature variations were no more than  $0.11 \text{ }^\circ\text{C min}^{-1}$ . 16 aliquots were averaged in total.  $\chi_{626}$  is concentration of the  $^{12}\text{C}^{16}\text{O}^{16}\text{O}$  isotopologue. Error bars for  $\Delta^{17}\text{O}_{\text{meas}}$  are  $1\sigma$ .

150 analogous to dual-inlet IRMS methods. This is done by filling V1 to 300 Torr of either  
 151 sample or reference gas, followed by expansion into the pre-evacuated optical cell (200 mL).  
 152 Each aliquot is measured in the optical cell for 40 seconds, during which the next aliquot  
 153 is filled into V1, before being evacuated and the next introduced. A measurement cycle,  
 154 defined as the measurement of subsequent aliquots of sample and reference gas, takes  $\sim 3$   
 155 minutes. Optical cell pressure is typically  $\sim 28 \text{ Torr}$ , and generally stable to  $<300 \text{ mTorr}$ .  
 156 Cell temperature is typically  $\sim 297 \text{ K}$  and stable within  $0.1 \text{ K}$  (Fig. 2). A complete analysis,  
 157 typically comprising of 18-20 measurement cycles, takes around 50 minutes. For all analyses,  
 158 the first 3 measurement cycles are ignored due to stabilization of temperature within the  
 159 optical cell.

160 From 31 March to 5 April lab aircon control malfunctioning was noted. During this period  
 161 it was identified that poor  $\Delta^{17}\text{O}$  precision was correlated to the rate of change of TILDAS  
 162 electronics temperature ( $dT/dt$ ). Samples analyzed between these dates were excluded as  
 163 the amplitude of  $dT/dt$  ( $A(dT/dt)$ ) was greater than  $0.11 \text{ }^\circ\text{C min}^{-1}$ , as evaluated by a 200-  
 164 second moving average. All other samples as reported in this study showed  $A(dT/dt) < 0.11$

165 °C min<sup>-1</sup> (see Supporting Information for further analysis of this effect).

## 166 Results and Discussion

### 167 Definition of Spectroscopic $\delta$ -values, and Concentration Dependence 168 due to Scale-Offset Errors.

169 Optical isotope spectrometers, such as our TILDAS instrument, determine  $\delta$ -values by mea-  
170 suring mole fractions of isotopologues.<sup>23</sup> Adopting IUPAC notation,<sup>24,25</sup> we can write, e.g.  
171 for the <sup>12</sup>C<sup>17</sup>O<sup>16</sup>O isotopologue:

$$\delta^{17}\text{O}_{\text{meas}} = \left( \frac{\chi_{627}/\chi_{626}}{X_{627}/X_{626}} - 1 \right) \times 1000 , \quad (1)$$

172 where the mole fraction,  $\chi_{627} = C_{627}V/n$ , is related to the measured concentration ( $C$ ) of the  
173 <sup>12</sup>C<sup>17</sup>O<sup>16</sup>O isotopologue in the optical cell (of volume,  $V$ ). Similar expressions can be derived  
174 for other isotopologues. For Aerodyne Research Inc. TILDAS instruments,  $X$  is the isotopo-  
175 logue abundance ratio (mol mol<sup>-1</sup>) as specified in the high-resolution transmission molecular  
176 absorption database (HITRAN), a standard database of *ab initio* atmospheric simulations.<sup>26</sup>  
177 In eq. (1),  $\chi$  is analogous to the isotope ratio of the sample, e.g. (<sup>17</sup>O/<sup>16</sup>O)<sub>sample</sub>, in the  
178 usual definition of an IRMS  $\delta$ -value, and  $X$  is analogous to the isotope ratio of the standard,  
179 (<sup>17</sup>O/<sup>16</sup>O)<sub>std</sub>. A  $\delta$ -value measured by spectroscopy (eq. 1) is thus not relative to a scale such  
180 as VPDB or VSMOW2-SLAP2, but rather, relative to HITRAN. Briefly, we also note that  
181 a spectroscopic  $\delta$ -value is technically a molecular abundance ratio, and not an atomic abun-  
182 dance ratio, as is measured by IRMS. However, it is assumed (for now) that the difference  
183 between the two is negligible.<sup>27</sup>

184 Because  $\delta$ -values measured by TILDAS are relative to HITRAN abundances, an extra  
185 step is needed to convert them to the VSMOW2-SLAP2 scale. A conversion procedure has  
186 previously been outlined to correct spectroscopic  $\delta^{13}\text{C}_{\text{meas}}$  for the offset from the VPDB

187 scale.<sup>23</sup> We extend this procedure to the triple oxygen isotope system (and VSMOW2-  
 188 SLAP2) as follows. Adopting the notation  $\chi'_{627} = \chi_{627}/X_{627}$ , we can modify eq. (1) thus:

$$\delta^{17}\text{O}_{\text{meas}} = \left( \frac{a_{627}\chi'_{627} + b_{627}}{a_{626}\chi'_{626} + b_{626}} - 1 \right) \times 1000 , \quad (2)$$

189 where  $a_{627}$ ,  $b_{627}$ ,  $a_{626}$ , and  $b_{626}$  are empirical scale factors which relate the HITRAN mole  
 190 fractions to the equivalent mole fractions on VSMOW2-SLAP2. We briefly note that there  
 191 are also instrument-specific responses that might result in apparent scale offsets. In this  
 192 case, the empirical factors in eq. (2) are expected to be unique to each instrumental setup.  
 193 Assuming  $A_{627} = a_{627}/a_{626}$ , and dropping the factor of 1000 for convenience, with further  
 194 modification it can be shown<sup>23</sup> that:

$$\delta^{17}\text{O}_{\text{std}} = \frac{\chi'_{626}}{A_{627}(\chi'_{626} - b_{626})} \left[ \delta^{17}\text{O}_{\text{meas}} + \frac{(A_{627}b_{626} - b_{627})}{\chi'_{626}} - A_{627} + 1 \right] . \quad (3)$$

195 This provides a general equation to correct TILDAS  $\delta$ -values to the VSMOW2-SLAP2 scale.  
 196 For interlaboratory carbonate standards, the value of  $\delta^{17}\text{O}_{\text{std}}$  is assumed (or is measured  
 197 by IRMS), and  $\delta^{17}\text{O}_{\text{meas}}$  and  $\chi_{626}$  are both then measured by TILDAS on multiple samples  
 198 of  $\text{CO}_2$  evolved from e.g. NBS18 and IAEA603 (mixed with dry  $\text{N}_2$ ). The constants  $A_{627}$ ,  
 199  $b_{627}$ , and  $b_{626}$  are then determined by non-linear least squares fitting to eq. (3). The same  
 200 procedure is then performed to correct  $\delta^{18}\text{O}_{\text{meas}}$  to  $\delta^{18}\text{O}_{\text{std}}$  (with constants  $A_{628}$ ,  $b_{628}$ , and  
 201  $b_{626}$ ). Note that if  $A_{627} = 1$  and  $b_{627}, b_{626} = 0$ , then eq. (3) reduces to  $\delta^{17}\text{O}_{\text{std}} = \delta^{17}\text{O}_{\text{meas}}$ ,  
 202 and the two scales are equal, as expected.

203 Significantly, eq. (3) shows that uncorrected TILDAS  $\delta$ -values will depend on the mea-  
 204 sured concentration of the most abundant  $^{12}\text{C}^{16}\text{O}^{16}\text{O}$  isotopologue ( $\chi'_{626}$ ). We call this effect  
 205 a “*concentration dependence due to scale-offset errors*”, because it arises as an arithmetic  
 206 consequence of the definition of the  $\delta$ -value (eq. 1), and because there are offsets between  
 207 HITRAN and VSMOW2-SLAP2 isotopologue abundance scales, and also instrument-specific  
 208 responses.

209 **Isotope Effects due to Diffusion of CO<sub>2</sub> During Sample Preparation.**

210 Our TILDAS protocol requires highly-repeatable dilutions of CO<sub>2</sub> in N<sub>2</sub> to trace concen-  
211 tration. However, if dilution is incomplete, and the sample is not very well mixed, isotope  
212 fractionation due to diffusion will be reflected in  $\delta^{17}\text{O}_{\text{meas}}$  and  $\delta^{18}\text{O}_{\text{meas}}$  values, in addition  
213 to concentration dependence (described above). Diffusion effects were found to be negligible  
214 in TILDAS measurements of the clumped isotopologue  $^{13}\text{C}^{16}\text{O}^{18}\text{O}$  (CO<sub>2</sub> in N<sub>2</sub> at 0.35%),  
215 due to cancellation of factors in the equation for the clumped equilibrium constant,  $K$ .<sup>19</sup>  
216 However, diffusion is likely to be more important in the triple oxygen isotope system, where  
217 very small differences in  $\delta^{17}\text{O}$  and  $\delta^{18}\text{O}$  propagate into large errors in  $(\Delta^{17}\text{O})$ .<sup>6</sup>

218 For triple oxygen isotopes, the relationship between fractionation factors during diffusion  
219 is defined<sup>6</sup> as  $\alpha^{17/16} = (\alpha^{18/16})^\theta$ , which, rearranging, gives:

$$\theta_{\text{diff}} = \frac{\ln(\alpha^{17/16})}{\ln(\alpha^{18/16})}. \quad (4)$$

220 Where the subscript “diff” indicates a diffusion process. For diffusion of CO<sub>2</sub> in N<sub>2</sub>, the  
221 binary diffusion coefficient can be calculated from Chapman-Enskog theory using:

$$D_{ab} = \frac{AT^{3/2}}{p\sigma_{ab}^2\Omega} \sqrt{\frac{m_a + m_b}{m_a m_b}}. \quad (5)$$

The subscripts  $a$  and  $b$  refer to the two gases,  $m$  is the molecular mass of each gas, and  
 $\sigma$  and  $\Omega$  are the average collision diameter (4.15 Å) and temperature dependent collision  
integral ( $\sim 1$ ), respectively. At 21 °C and 700 mbar,  $D$  is 0.1879 cm<sup>2</sup> s<sup>-1</sup>. eq. (5) can  
be modified to describe the ratios of isotopologue concentrations, and thereby related to  
fractionation factors. With further algebra, common terms such as  $T$ ,  $p$ , etc. will cancel,  
and it can be shown that the ratio of fractionation factors is just the ratio of diffusivities for

each isotopologue:

$$\begin{aligned}
 \theta_{\text{diff}} &= \frac{\ln\left(\frac{D_{45,28}}{D_{44,28}}\right)}{\ln\left(\frac{D_{46,28}}{D_{44,28}}\right)} \\
 &= \frac{\ln\left(\frac{44}{45}\right) + \ln\left(\frac{45+28}{44+28}\right)}{\ln\left(\frac{44}{46}\right) + \ln\left(\frac{46+28}{44+28}\right)} \\
 &= 0.509
 \end{aligned}$$

222 According to the conventional  $\delta$ -notation definition of the triple oxygen isotope system,

$$\Delta^{17}\text{O} \equiv \delta^{17}\text{O} - \theta\delta^{18}\text{O} , \tag{6}$$

223 where  $\theta = 0.528$  (global reference line) and  $\delta^{17}\text{O} = 1000\ln(\delta^{17}\text{O}/1000 + 1)$ , and a similar  
 224 expression exists for  $\delta^{18}\text{O}$ . Hence, the mass-dependent fractionation exponent,  $\theta$ , is lower for  
 225 diffusion than for the global reference line. When  $\text{CO}_2$  diffuses in  $\text{N}_2$ ,  $\delta^{18}\text{O}$  and  $\delta^{17}\text{O}$  values  
 226 will be shifted lower relative to their original values (i.e. relative to the pure  $\text{CO}_2$ ). This  
 227 gas will also tend to be under-diluted with respect to the target concentration ( $400 \mu\text{mol}$   
 228  $\text{mol}^{-1}$ ). And by mass balance,  $\delta^{18}\text{O}$  and  $\delta^{17}\text{O}$  values of the remaining (un-mixed)  $\text{CO}_2$  will  
 229 be shifted higher.

230 A framework for errors due to diffusion, as well as scale-offset, is shown in Fig. 3A for a  
 231 hypothetical gas with a true value of  $\Delta^{17}\text{O}_{\text{meas}} = 0$ . If the sample gas is well-mixed, with  
 232 no diffusion, and no offset error, then all aliquots would be measured along a line of slope  
 233  $\theta = 0.528$  in  $\delta^{17}\text{O}_{\text{meas}}-\delta^{18}\text{O}_{\text{meas}}$  space. Samples with scale-offset error would lie along a curve  
 234 (shown in red) depending on the measured concentration of  $^{12}\text{C}^{16}\text{O}^{16}\text{O}$  ( $\chi'_{626}$ , eq. 3), as well  
 235 as the values of  $A_{627}$ ,  $A_{628}$ , etc. In addition, if there are diffusion effects, then individual  
 236 aliquots will lie along a slope of  $\theta = 0.509$  (shown in blue). In reality, the two effects occur  
 237 together, so that the total error,  $\varepsilon(\Delta^{17}\text{O})$ , is the sum of errors due to scale offset,  $\varepsilon(\text{scale})$ ,  
 238 and diffusion,  $\varepsilon(\text{diff})$ . Aliquots of higher concentration will be found above the true slope,  
 239 and lower concentrations below it, resulting in a ‘‘cone’’ of scatter, with an average gradient

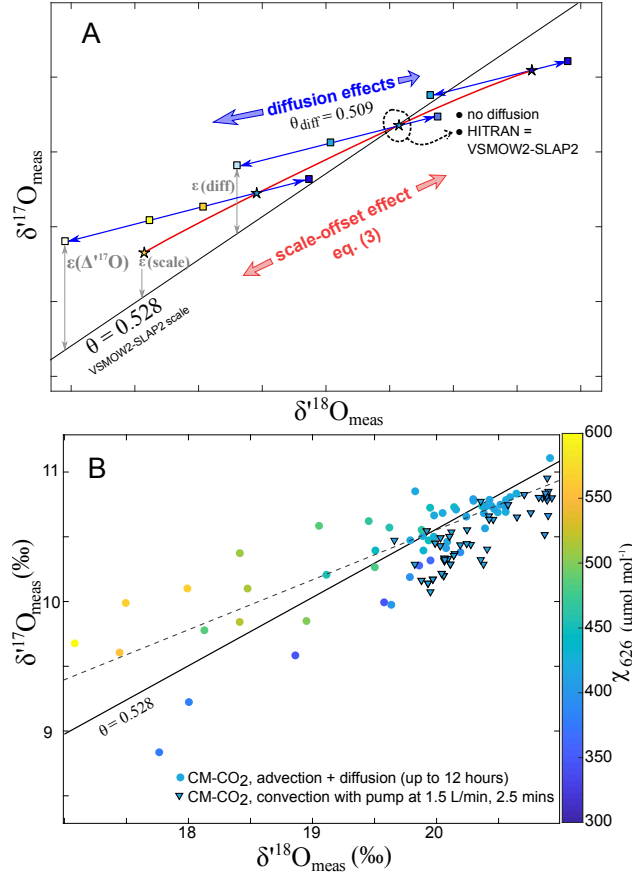


Figure 3: (A) Graphical framework for errors in TILDAS measurements of triple oxygen isotope composition of CO<sub>2</sub> (see further discussion in text). Stars are samples of different target concentration. Squares are aliquots drawn from each sample (under- or over-diluted). (B) shows the effects of incomplete mixing of CO<sub>2</sub> in N<sub>2</sub> on  $\delta^{17}\text{O}_{\text{meas}}$  and  $\delta^{18}\text{O}_{\text{meas}}$ . Filled triangles show multiple aliquots from 4 samples of CO<sub>2</sub> evolved from an internal standard, Cavendish Marble (CM), circulated by diaphragm pump (Parker CTS) for 2.5 minutes to allow proper mixing before measurement. Other datapoints are aliquots from five samples of CM, mixed only by advection and diffusion (for up to 12 hours).

240 lower than  $\theta = 0.528$  (and erroneously high  $\Delta^{17}\text{O}_{\text{meas}}$  values).

241 To test this framework, we conducted an experiment on samples with and without our  
 242 circulating pump, using CO<sub>2</sub> from  $\sim 0.8$  mg samples of an internal laboratory standard,  
 243 Cavendish Marble (CM-CO<sub>2</sub>). 5 samples were mixed into MV1,2,3 by turbulent advection  
 244 and diffusion only, without the circulating pump. The time taken for diffusive mixing was  
 245 varied on a sample-by-sample basis from  $\sim 10$  minutes to 12 hours. In addition, the average  
 246  $\chi'_{626}$  of each sample varied from 400 to 466  $\mu\text{mol mol}^{-1}$ . 4 samples of the same material were

247 mixed for  $\sim 2.5$  minutes with the pump, immediately after turbulent advection.  $\chi'_{626}$  of these  
248 samples varied from 368 to 405  $\mu\text{mol mol}^{-1}$ .

249 For the samples unmixed by pump, Fig. 3B shows good agreement with the framework in  
250 Fig. 3A. Aliquots from all samples form a cone of scatter, with an average slope (dashed line)  
251 lower than  $\theta = 0.528$ . Better-mixed aliquots, close to the target concentration range, cluster  
252 more closely to  $\theta = 0.528$ . When the circulating pump is added (filled triangles), all aliquots  
253 have an average slope very near  $\theta = 0.528$ . Without the pump,  $1\sigma$  sample repeatability  
254 for  $\Delta^{17}\text{O}_{\text{meas}}$  was  $30 \pm 130$  per meg, and aliquot repeatability for  $\chi'_{626}$  was between 4 and  
255 80  $\mu\text{mol mol}^{-1}$ . With the pump, sample repeatability for  $\Delta^{17}\text{O}_{\text{meas}}$  improved substantially  
256 to  $-230 \pm 10$  per meg, in significantly less time ( $\sim 2.5$  minutes vs hours). With the pump,  
257 aliquot repeatability for  $\chi'_{626}$  was also excellent (between 0.4 and 0.9  $\mu\text{mol mol}^{-1}$ ). This  
258 result supports the conclusion that, without proper mixing, diffusion effects can be very  
259 significant in sample preparation, necessitating very long times for well-mixed sample gases,  
260 prior to TILDAS measurements of  $\Delta^{17}\text{O}$ . Promisingly, forced convection via circulating loop  
261 solves these issues. Preparation of the entire sample gas prior to measurement (as opposed  
262 to aliquot-by-aliquot basis) also provides a useful check on the extent of mixing, which may  
263 be evaluated by aliquot repeatability of  $\chi'_{626}$ .

## 264 Correction of Spectroscopic $\delta^{17}\text{O}$ and $\delta^{18}\text{O}$ values to the VSMOW2- 265 SLAP2 Scale.

266 In what follows, we compare triple oxygen isotope measurements both without correction  
267 ( $\delta^{17}\text{O}_{\text{meas}}$ ,  $\delta^{18}\text{O}_{\text{meas}}$ ), and corrected to VSMOW2-SLAP2 ( $\delta^{17}\text{O}_{\text{corr}}$ ,  $\delta^{18}\text{O}_{\text{corr}}$ ). These data  
268 are shown in Table 1. All samples were well-mixed by circulating pump for 2.5 minutes prior  
269 to TILDAS measurement (described in detail above). For conciseness, corresponding  $\delta^{13}\text{C}$   
270 data for these samples are reported in the Supporting Information. For the correction, we  
271 used interlaboratory carbonate standards IAEA603 ( $n = 6$ ), and NBS18 ( $n = 4$ ). Assuming  
272 VSMOW2-SLAP2 values for  $\text{CO}_2$  from IAEA603 and NBS18 given by Wostbrock *et al.*,<sup>12</sup> we

273 fitted eq. (3) to all aliquots of  $\delta^{17}\text{O}_{\text{meas}}$ , and  $\chi'_{626}$ , in MATLAB. The same procedure was then  
274 performed for  $\delta^{18}\text{O}_{\text{meas}}$ . For  $\delta^{17}\text{O}$ , the fitted parameters were:  $A_{627} = 0.674$ ,  $b_{627} = -1974$ ,  
275  $b_{626} = -168$ ,  $R^2 = 0.999$ ; and for  $\delta^{18}\text{O}$ , they were  $A_{628} = 0.632$ ,  $b_{628} = -3782$ ,  $b_{626} = -207$ ,  
276  $R^2 = 0.999$ .

277 We have corrected our  $\delta$ -values to the VSMOW2-SLAP2 scale using previously-published  
278 values for carbonate standards from an IRMS method<sup>12</sup> because this particular method is  
279 regarded as a relatively assumption-free for triple oxygen isotope analysis.<sup>28</sup> A more nuanced  
280 approach, for future investigation, would be to perform equilibrations between  $\text{CO}_2$  and  
281 VSMOW2, SLAP2 water directly on our cart within MV3, thereafter trapping and analyzing  
282 the equilibrated  $\text{CO}_2$ . Another alternative is to correct our working reference gas directly  
283 to VSMOW2-SLAP2.<sup>23</sup> In our procedure, we avoid calibrating our working reference gas  
284 because (1) it is used merely to correct for short-term drift in  $\delta$ -values between aliquots,  
285 and (2) because long-term drift might occur as our 50L tank empties (for instance, due to  
286 potential effusion effects).

287 Although we also report NBS19 ( $n = 7$ ) in this table, it was excluded from the fitting  
288 because these samples had substantially worse reproducibility for  $\Delta^{17}\text{O}_{\text{corr}}$  ( $1\sigma = 60$  per  
289 meg,  $n = 7$ ). Although the experimental conditions for all standard samples were identical,  
290 we used an almost-empty vial of NBS19, whereas a fresh vial of IAEA603 was opened for  
291 this experiment. We suggest that the significantly greater degree of scatter in NBS19 might  
292 be related to slight but significant exchange of this standard with moisture in this old vial,  
293 over  $\sim 30$  years of regular use, a phenomenon discussed by other authors.<sup>29</sup>

294 Reproducibility of  $\Delta^{17}\text{O}$  was significantly improved by correction to VSMOW2-SLAP2  
295 using eq. (3), for IAEA603 and NBS19. After correction, reproducibility of IAEA603 im-  
296 proved significantly from 7 per meg (1 SE) to 4 per meg; NBS19 also improved from 25 to  
297 21 per meg. Reproducibility of NBS18 was similar before and after correction, at  $\sim 10$  per  
298 meg. The reproducibility of our  $\delta^{17}\text{O}_{\text{corr}}$  and  $\delta^{18}\text{O}_{\text{corr}}$  values for IAEA603 (7 and 19 per meg,  
299 respectively), are significantly improved over previously-published TILDAS measurements of



Table 1: Triple oxygen isotope data for CO<sub>2</sub> evolved by phosphoric acid digestion of inter-laboratory carbonate standards at 70°C, measured by TILDAS. Between 13 and 18 aliquots were measured per sample ( $\sim 0.9$  mg total carbonate).  $\delta^{17}\text{O}$  and  $\delta^{18}\text{O}$  values from individual aliquots are corrected to the VSMOW2-SLAP2 scale using the IAEA603 (CO<sub>2</sub>) and NBS18 (CO<sub>2</sub>) values of Wostbrock et al. (2020). The corrected values,  $\delta^{17}\text{O}_{\text{corr}}$  and  $\delta^{18}\text{O}_{\text{corr}}$ , were then used to calculate  $\Delta^{17}\text{O}_{\text{corr}}$ .  $\chi_{626}$  is the concentration of the  $^{12}\text{C}^{16}\text{O}^{16}\text{O}$  isotopologue in each sample,  $\mu\text{mol}\cdot\text{mol}^{-1}$ , with  $1\sigma$  repeatability of aliquots in parentheses. All isotope data are ‰, with the exception of  $\Delta^{17}\text{O}_{\text{corr}}$ , which are per meg,  $\theta = 0.528$ .

Sample	$\chi_{626}$	$\delta^{17}\text{O}^a$	$\delta^{18}\text{O}^a$	$\delta^{17}\text{O}_{\text{corr}}^b$	$\delta^{18}\text{O}_{\text{corr}}^b$	$\Delta^{17}\text{O}_{\text{corr}}$
IAEA603-4	393.3(0.5)	14.311	27.560	20.036	38.250	-158
IAEA603-5	404.8(0.6)	14.290	27.435	20.045	38.220	-140
IAEA603-6	412.8(0.8)	14.288	27.471	20.097	38.374	-161
IAEA603-7	393.8(0.8)	14.287	27.493	20.012	38.181	-147
IAEA603-9	405.3(0.7)	14.277	27.435	20.034	38.224	-149
IAEA603-10	415.6(0.7)	14.216	27.300	20.000	38.172	-158
<b>Average</b>		<b>14.291</b>	<b>27.479</b>	<b>20.037</b>	<b>38.237</b>	<b>-151</b>
$\pm 1\sigma$		<b>0.013</b>	<b>0.052</b>	<b>0.015</b>	<b>0.043</b>	<b>10</b>
<b>St. err<sup>c</sup></b>		<b>0.006</b>	<b>0.023</b>	<b>0.007</b>	<b>0.019</b>	<b>4</b>
NBS18-8	397.7(0.4)	3.605	6.925	8.941	17.148	-113
NBS18-12	409.6(0.5)	3.791	7.374	9.075	17.389	-106
NBS18-13	405.1(0.5)	3.840	7.409	9.150	17.463	-71
NBS18-14	401.8(0.9)	3.763	7.313	9.112	17.461	-107
<b>Average</b>		<b>3.750</b>	<b>7.255</b>	<b>9.070</b>	<b>17.365</b>	<b>-99</b>
$\pm 1\sigma$		<b>0.102</b>	<b>0.224</b>	<b>0.091</b>	<b>0.149</b>	<b>19</b>
<b>St. err<sup>c</sup></b>		<b>0.051</b>	<b>0.112</b>	<b>0.046</b>	<b>0.074</b>	<b>10</b>
NBS19-5	401.4(0.6)	14.164	27.295	19.895	38.052	-196
NBS19-6	409.0(0.6)	14.269	27.435	20.0533	38.266	-151
NBS19-7	397.6(0.5)	14.244	27.500	19.9783	38.222	-203
NBS19-11	397.3(0.7)	14.406	27.796	20.146	38.524	-195
NBS19-12	388.5(0.7)	14.492	27.868	20.208	38.515	-127
NBS19-13	411.3(0.5)	14.443	27.678	20.224	38.530	-120
NBS19-14	416.6(0.7)	14.418	27.798	20.184	38.582	-177
<b>Average</b>		<b>14.348</b>	<b>27.624</b>	<b>20.098</b>	<b>38.385</b>	<b>-150</b>
$\pm 1\sigma$		<b>0.122</b>	<b>0.217</b>	<b>0.126</b>	<b>0.203</b>	<b>60</b>
<b>St. err<sup>c</sup></b>		<b>0.046</b>	<b>0.081</b>	<b>0.048</b>	<b>0.077</b>	<b>22</b>

<sup>a</sup> Molecular abundance ratios by spectroscopy, e.g.  $\delta(627)$  are assumed equal to atomic abundance ratios, e.g.  $\delta^{17}\text{O}$ , and the atomic notation is retained; <sup>b</sup> Corrected using eq. (3);

<sup>c</sup> Standard error =  $1\sigma/\sqrt{n}$

300 isotopologue ratios of CO<sub>2</sub> (reproducibilities of 30 and 40 per meg for <sup>17</sup>O/<sup>16</sup>O and <sup>18</sup>O/<sup>16</sup>O,  
 301 respectively).<sup>20,21</sup> Reproducibilities for NBS18 and NBS19 are a similar order of magnitude  
 302 to these measurements. These results further emphasise the importance of correcting for  
 303 scale-offset effects, at least for some samples, and provides a relatively simple strategy for  
 304 correcting spectroscopic  $\delta$ -values to VSMOW2-SLAP2.

### 305 Utility of high-precision $\Delta^{17}\text{O}$ (CO<sub>2</sub>) TILDAS measurements in com- 306 parison to IRMS.

307 Mean  $\Delta^{17}\text{O}_{\text{corr}}$  values of IAEA603, NBS18, and NBS19 by TILDAS are internally consistent  
 308 with Wostbrock *et al.*,<sup>12</sup> and are in excellent agreement with other high-precision IRMS  
 309 methods which rely on conversion of CO<sub>2</sub> to O<sub>2</sub><sup>9,30</sup> to within 1 SE reproducibility (Fig. 4).  
 310 Encouragingly, our methodology requires substantially less sample ( $\sim 0.9$  mg of carbonate)  
 311 compared to all current IRMS methods (typically 5-10 mg).<sup>9,12,29,30</sup> In addition, TILDAS  
 312 requires somewhat less complicated sample preparation and shorter measurement times than  
 313 IRMS. Furthermore, the internal consistency between our results and IRMS supports the  
 314 assumption that differences between atomic and molecular abundance ratios are negligible,  
 315 at this level of reproducibility.

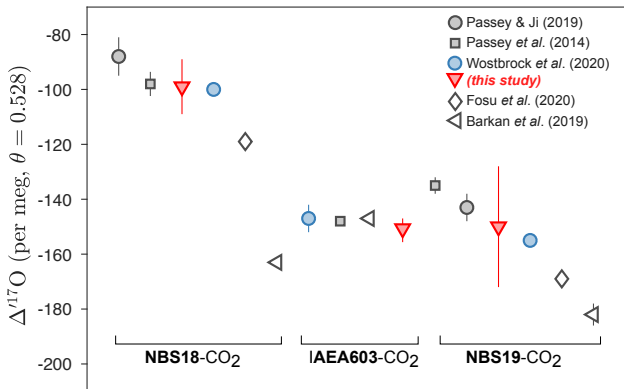


Figure 4: Comparison between TILDAS (red triangles, this study) and IRMS measurements of  $\Delta^{17}\text{O}$ , for CO<sub>2</sub> evolved from Interlaboratory Standards. Errorbars denote 1 SE. Filled grey symbols denote conversion methods (CO<sub>2</sub> to O<sub>2</sub>, or direct BrF<sub>5</sub> fluorination of carbonate). Open symbols indicate methods reliant on platinum-catalyzed exchange of CO<sub>2</sub> with O<sub>2</sub>.

316 One challenge of our method is the requirement that samples are very well-mixed. How-  
317 ever, mixing the sample prior to measurement (as opposed to on a per aliquot basis), means  
318 that the degree of mixing is easily evaluated from successive measurements of aliquot concen-  
319 tration(s). We also note that there is significant disagreement between some IRMS methods  
320 of triple oxygen analysis (see Fig. 4).<sup>28</sup> Typically, methods that rely on platinum-catalyzed  
321 exchange of CO<sub>2</sub> with O<sub>2</sub><sup>14,15,29</sup> have systematically lower  $\Delta^{17}\text{O}$  values than conversion  
322 methods. Our  $\Delta^{17}\text{O}$  values are corrected to values from a conversion method, and are  
323 therefore in disagreement with exchange methods, with the exception of NBS19, which, to  
324 within its large uncertainty, agrees with most methods. Because this problem seems to be  
325 unique to our NBS19, we argue that these errors are likely related to sample heterogeneity  
326 and contamination issues (discussed above). The result underscores the importance of using  
327 carefully-chosen standards in triple oxygen isotope research, for which future interlaboratory  
328 comparison is warranted.

## 329 Conclusions

330 We have presented a method for triple oxygen isotope analysis by TILDAS, with a sample  
331 reproducibility for  $\Delta^{17}\text{O}$  of CO<sub>2</sub> from interlaboratory carbonate standards that equals that  
332 of current high-precision IRMS methods (provided the sample is well-mixed in N<sub>2</sub>). Our  
333 method brings several additional advantages, such as smaller sample size (e.g.  $\sim 0.9$  mg of  
334 carbonate), increased throughput, and direct measurement of  $\Delta^{17}\text{O}$  in CO<sub>2</sub>. In addition,  
335 our system is readily modifiable. It is able to handle several different sources of CO<sub>2</sub>, e.g.  
336 via Gasbench acid digestion, break-seal vials, or dry atmospheric samples collected in our re-  
337 movable flask ( $\sim 586$  mL). We have set out a simple procedure for the correction of TILDAS  
338  $\delta$ -values to the VSMOW2-SLAP2 scale. Future work will allow for more direct calibration  
339 via equilibration of CO<sub>2</sub> with VSMOW2 and SLAP2 waters, and combine TILDAS mea-  
340 surements of  $\Delta^{17}\text{O}$  with multiply-substituted CO<sub>2</sub> isotopologues,<sup>19</sup> so that  $\delta^{17}\text{O}$ ,  $\delta^{18}\text{O}$ , and

341  $\delta_{47}$  of the same sample are measured simultaneously. We expect this, or similar techniques,  
342 to have significant impact on future atmospheric monitoring and terrestrial (paleo)climate  
343 research.

## 344 Supporting Information

345 Supporting Information: Additional experimental details, including photographs of experi-  
346 mental setup, and LabVIEW and ECL code (PDF).

## 347 Acknowledgement

348 This work was funded by the South African Biogeochemistry National Research Infrastruc-  
349 ture Platform (BIOGRIP), and a Launching Grant from the University of Cape Town, as well  
350 as a grant from the National Research Foundation of South Africa (120806). VJH thanks  
351 Ben Passey and Naomi Levin for hosting him at the University of Michigan  $\Delta^{17}\text{O}$  line,  
352 kindly facilitated by Tyler Faith, and Dave Braun (NSF Grant 1826666). Scott Blumenthal  
353 is thanked for helpful comments on the manuscript, and Shuhei Ono is thanked for support  
354 and comments in the early conception of this project.

## 355 References

- 356 (1) Thiemens, M. H.; Jackson, T.; Zipf, E. C.; Erdman, P. W.; van Egmond, C. Carbon  
357 dioxide and oxygen isotope anomalies in the mesosphere and stratosphere. *Science*  
358 **1995**, *270*, 969–972.
- 359 (2) Boering, K.; Jackson, T.; Hoag, K.; Cole, A.; Perri, M.; Thiemens, M.; Atlas, E.  
360 Observations of the anomalous oxygen isotopic composition of carbon dioxide in the  
361 lower stratosphere and the flux of the anomaly to the troposphere. *Geophys. Res. Lett.*  
362 **2004**, *31*.

- 363 (3) Yeung, L. Y.; Affek, H. P.; Hoag, K. J.; Guo, W.; Wiegel, A. A.; Atlas, E. L.; Schauf-  
364 fler, S. M.; Okumura, M.; Boering, K. A.; Eiler, J. M. Large and unexpected en-  
365 richment in stratospheric  $^{16}\text{O}^{13}\text{C}^{18}\text{O}$  and its meridional variation. *PNAS* **2009**, *106*,  
366 11496–11501.
- 367 (4) Yang, J.-W.; Brandon, M.; Landais, A.; Duchamp-Alphonse, S.; Blunier, T.; Prié, F.;  
368 Extier, T. Global biosphere primary productivity changes during the past eight glacial  
369 cycles. *Science* **2022**, *375*, 1145–1151.
- 370 (5) Hoag, K.; Still, C.; Fung, I.; Boering, K. Triple oxygen isotope composition of tropo-  
371 spheric carbon dioxide as a tracer of terrestrial gross carbon fluxes. *Geophys. Res. Lett.*  
372 **2005**, *32*.
- 373 (6) Miller, M. F.; Pack, A. Why measure  $^{17}\text{O}$ ? Historical perspective, triple-isotope sys-  
374 tematics and selected applications. *Rev. Mineral. Geochem.* **2021**, *86*, 1–34.
- 375 (7) Hofmann, M.; Horváth, B.; Schneider, L.; Peters, W.; Schützenmeister, K.; Pack, A.  
376 Atmospheric measurements of  $\Delta^{17}\text{O}$  in  $\text{CO}_2$  in Göttingen, Germany reveal a seasonal  
377 cycle driven by biospheric uptake. *Geochim. Cosmochim. Acta* **2017**, *199*, 143–163.
- 378 (8) Bao, H.; Lyons, J.; Zhou, C. Triple oxygen isotope evidence for elevated  $\text{CO}_2$  levels  
379 after a Neoproterozoic glaciation. *Nature* **2008**, *453*, 504–506.
- 380 (9) Passey, B. H.; Hu, H.; Ji, H.; Montanari, S.; Li, S.; Henkes, G. A.; Levin, N. E. Triple  
381 oxygen isotopes in biogenic and sedimentary carbonates. *Geochim. Cosmochim. Acta*  
382 **2014**, *141*, 1–25.
- 383 (10) Gehler, A.; Gingerich, P. D.; Pack, A. Temperature and atmospheric  $\text{CO}_2$  concentra-  
384 tion estimates through the PETM using triple oxygen isotope analysis of mammalian  
385 bioapatite. *PNAS* **2016**, *113*, 7739–7744.

- 386 (11) Lehmann, S. B.; Levin, N. E.; Passey, B. H.; Hu, H.; Cerling, T. E.; Miller, J. H.;  
387 Arppe, L.; Beverly, E. J.; Hoppe, K. A.; Huth, T. E., et al. Triple oxygen isotope  
388 distribution in modern mammal teeth and potential geologic applications. *Geochim.*  
389 *Cosmochim. Acta* **2022**,
- 390 (12) Wostbrock, J. A.; Cano, E. J.; Sharp, Z. D. An internally consistent triple oxygen  
391 isotope calibration of standards for silicates, carbonates and air relative to VSMOW2  
392 and SLAP2. *Chem. Geol.* **2020**, *533*, 119432.
- 393 (13) Mahata, S.; Bhattacharya, S.; Wang, C.-H.; Liang, M.-C. Oxygen isotope exchange  
394 between O<sub>2</sub> and CO<sub>2</sub> over hot platinum: An innovative technique for measuring  $\Delta^{17}\text{O}$   
395 in CO<sub>2</sub>. *Anal. Chem.* **2013**, *85*, 6894–6901.
- 396 (14) Fosu, B. R.; Subba, R.; Peethambaran, R.; Bhattacharya, S.; Ghosh, P. Developments  
397 and applications in triple oxygen isotope analysis of carbonates. *ACS Earth Space*  
398 *Chem.* **2020**, *4*, 702–710.
- 399 (15) Barkan, E.; Musan, I.; Luz, B. High-precision measurements of  $\delta^{17}\text{O}$  and  $^{17}\text{O}_{\text{excess}}$  of  
400 NBS19 and NBS18. *Rapid Commun. Mass Spectrom.* **2015**, *29*, 2219–2224.
- 401 (16) Barkan, E.; Luz, B. High-precision measurements of  $^{17}\text{O}/^{16}\text{O}$  and  $^{18}\text{O}/^{16}\text{O}$  ratios in  
402 CO<sub>2</sub>. *Rapid Commun. Mass Spectrom.* **2012**, *26*, 2733–2738.
- 403 (17) Genoud, G.; Vainio, M.; Phillips, H.; Dean, J.; Merimaa, M. Radiocarbon dioxide  
404 detection based on cavity ring-down spectroscopy and a quantum cascade laser. *Opt.*  
405 *Lett.* **2015**, *40*, 1342–1345.
- 406 (18) Ono, S.; Wang, D. T.; Gruen, D. S.; Sherwood Lollar, B.; Zahniser, M. S.; Mc-  
407 Manus, B. J.; Nelson, D. D. Measurement of a doubly substituted methane isotopologue,  
408  $^{13}\text{CH}_3\text{D}$ , by tunable infrared laser direct absorption spectroscopy. *Anal. Chem.* **2014**,  
409 *86*, 6487–6494.

- 410 (19) Wang, Z.; Nelson, D. D.; Dettman, D. L.; McManus, J. B.; Quade, J.; Hunting-  
411 ton, K. W.; Schauer, A. J.; Sakai, S. Rapid and Precise Analysis of Carbon Dioxide  
412 Clumped Isotopic Composition by Tunable Infrared Laser Differential Spectroscopy.  
413 *Anal. Chem.* **2019**, *92*, 2034–2042.
- 414 (20) Sakai, S.; Matsuda, S.; Hikida, T.; Shimono, A.; McManus, J. B.; Zahniser, M.; Nel-  
415 son, D.; Dettman, D. L.; Yang, D.; Ohkouchi, N. High-Precision Simultaneous  $^{18}\text{O}/^{16}\text{O}$ ,  
416  $^{13}\text{C}/^{12}\text{C}$ , and  $^{17}\text{O}/^{16}\text{O}$  Analyses for Microgram Quantities of  $\text{CaCO}_3$  by Tunable In-  
417 frared Laser Absorption Spectroscopy. *Anal. Chem.* **2017**, *89*, 11846–11852.
- 418 (21) Sakai, S.; Otsuka, T.; Matsuda, S.; Sakairi, Y.; Uchida, R.; Sugahara, K.; Kano, A.;  
419 Yang, D. Subnanomolar Sensitive Stable Isotopic Determination in  $\text{CO}_2$  by Tunable  
420 Infrared Laser Absorption Spectroscopy. *Anal. Chem.* **2022**, *94*, 6446–6450.
- 421 (22) McManus, J. B.; Nelson, D. D.; Zahniser, M. S. Design and performance of a dual-laser  
422 instrument for multiple isotopologues of carbon dioxide and water. *Opt. Express* **2015**,  
423 *23*, 6569–6586.
- 424 (23) Griffith, D.; Deutscher, N.; Caldow, C.; Kettlewell, G.; Riggensbach, M.; Hammer, S. A  
425 Fourier transform infrared trace gas and isotope analyser for atmospheric applications.  
426 *Atmos. Meas. Tech.* **2012**, *5*, 2481–2498.
- 427 (24) Cohen, E. R.; Cvitaš, T.; Frey, J. G.; Holmström, B.; Kuchitsu, K.; Marquardt, R.;  
428 Mills, I.; Pavese, F.; Quack, M.; Stohner, J., et al. *Quantities, units and symbols in*  
429 *physical chemistry*; IUPAC, 2007.
- 430 (25) Coplen, T. B. *Explanatory glossary of terms used in expression of relative isotope ratios*  
431 *and gas ratios*; IUPAC, 2008.
- 432 (26) Rothman, L. S.; Jacquemart, D.; Barbe, A.; Benner, D. C.; Birk, M.; Brown, L.;  
433 Carleer, M.; Chackerian Jr, C.; Chance, K.; Coudert, L. e. a., et al. The HITRAN

- 434 2004 molecular spectroscopic database. *J. Quant. Spectrosc. Radiat. Transf.* **2005**, *96*,  
435 139–204.
- 436 (27) Kerstel, E. *Handbook of stable isotope analytical techniques*; Elsevier, 2004; pp 759–787.
- 437 (28) Passey, B. H.; Levin, N. E. Triple oxygen isotopes in meteoric waters, carbonates,  
438 and biological apatites: implications for continental paleoclimate reconstruction. *Rev.*  
439 *Mineral. Geochem.* **2021**, *86*, 429–462.
- 440 (29) Barkan, E.; Affek, H. P.; Luz, B.; Bergel, S. J.; Voarintsoa, N. R. G.; Musan, I. Cali-  
441 bration of  $\delta^{17}\text{O}$  and  $^{17}\text{O}_{\text{excess}}$  values of three international standards: IAEA-603, NBS19  
442 and NBS18. *Rapid Commun. Mass Spectrom.* **2019**, *33*, 737.
- 443 (30) Passey, B. H.; Ji, H. Triple oxygen isotope signatures of evaporation in lake waters and  
444 carbonates: A case study from the western United States. *EPSL* **2019**, *518*, 1–12.

## 445 Supporting Information

### 446 1. Photographs





Figure 5: Photograph of the TILDAS instrument (lasers housed inside black box), with automated valve sampling system (top), and custom-built cart for automated CO<sub>2</sub> extraction and dilution (below).

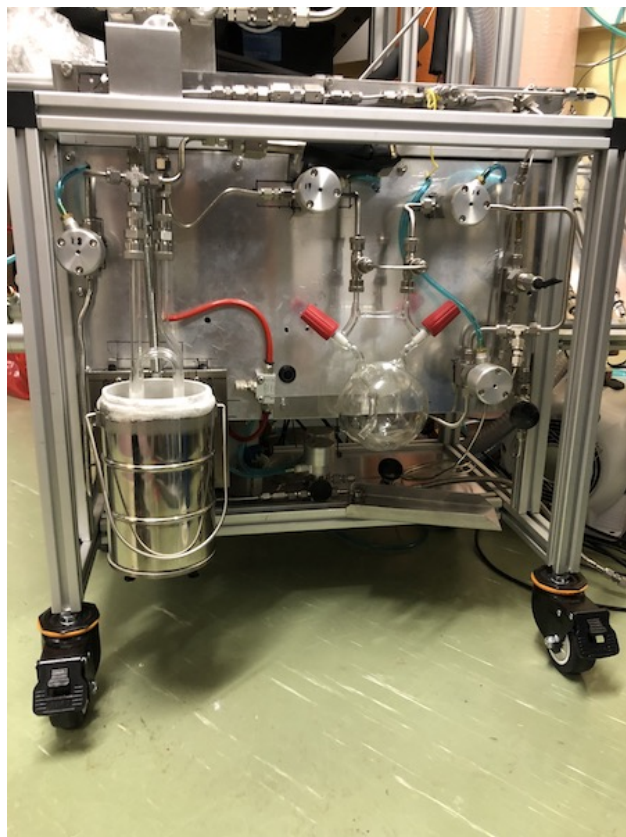


Figure 6: Photograph of the custom-built cart for automated CO<sub>2</sub> extraction and dilution. A pneumatically-operated dewar of liquid Nitrogen (left) is shown in the “up” position whilst CO<sub>2</sub> is actively trapped in MV2.



Figure 7: Photograph of MV1, the custom-built sampling flask (GlassChem cc, South Africa). Two teflon stopcocks (either Schott Produran or J. Young) seal off a  $\sim 586$  mL round-bottomed borosilicate flask. A siphon ensures efficient flow through the volume. The flask can be disconnected from two Ultra-Torr quick connects (Swagelok). Valves 17 and 16 are shown to the left and right of the flask, respectively. A short tube of  $1/8$ " diameter acts as a bypass for the flask. All other tubes are  $1/4$ ". The piece of horizontal glass on the flask parallel to this bypass tube is solid, and is used to carry the flask when disconnected from the autocart. A design drawing for the flask can be obtained from the author upon request.

## 447 2. dT/dt Experiments

### 448 Summary and Results

449 To address the effects of temperature on TILDAS analytical precision a series of reference  
450 gas vs. reference gas experiments were conducted. Over the course of a day, repeated  
451 analyses (each with a duration between 38 and 65 minutes) of reference gas against itself  
452 were performed while varying multiple aspects of the TILDAS operational environment.  
453 In a theoretically perfect system, all  $\Delta^{17}\text{O}$  values would equal 0. Tested variables were  
454 internal  $\text{N}_2$  purge rate, lab aircon temperature setpoint, and the absence altogether of aircon  
455 temperature control, as summarized in Table A1.

Table 2: Experimental Conditions

Experiment	Time started	Duration (min)	$\text{N}_2$ purge (L/min)	Aircon setpoint ( $^{\circ}\text{C}$ )
1	6:31	65	1.5	23
2	7:38	60	1	23
3	8:59	38	1.5	23
4	10:02	60	1	23
5	11:11	45	1	23
6	12:11	57	1.5	23
7	13:31	55	1	23
8	14:34	47	1	23
9	15:30	45	1	OFF
10	16:39	41	1	24
11	17:44	52	1	OFF

456 Variety in the internal purge rate was not expected to have a large influence on measure-  
457 ment precision. Other than the potential impact on the thermal stability of the TILDAS  
458 housing, purge rate is taken to be inconsequential providing that it is sufficient to maintain a  
459 dry,  $\text{N}_2$  dominated internal environment. As observed, the purge  $\text{N}_2$  flow rate had negligible  
460 observable effect on analytical performance over the course of the experiments.

461 Several key aspects of the TILDAS system are controlled for and influenced by temper-  
462 ature. Laser temperatures are regulated by a liquid chiller with milli-Kelvin scale precision.  
463 The instrument used in this project uses the liquid chiller set to  $23^{\circ}\text{C}$ . As the liquid tem-

464 perature is maintained by a fan blowing air across the coolant liquid, lab aircon setpoint  
 465 is likely to have an impact on coolant temperature stability. To ease the work load of the  
 466 chiller lab aircon temperature was set to 23°C for a majority of the following experiments.  
 467 The effects of lab air temperature on measurement precision were tested by occasionally  
 468 shutting off the aircon unit (Experiments 9, 11) and increasing the temperature setpoint (to  
 469 (24°C, Experiment 10). Previous observations not documented here revealed that an aircon  
 470 setpoint matching the chiller temperature (23°C), provided greater coolant stability than a  
 471 setpoint just below (22°C). However, no correlated change in measured analytical precision  
 472 was observed and laser temperature stability was unaffected.

473 To access the impacts of electronics temperature on measurement precision, the rate of  
 474 change of the temperature ( $dT/dt$ , °C min<sup>-1</sup>) of the electronics was mapped using a 200-  
 475 second moving average. The curve produced from this moving average was plotted alongside  
 476 calculated  $\Delta^{17}\text{O}$  values for each measured reference gas vs. reference gas measurement  
 477 cycle. A clear trend is observed correlating the amplitude (A) of the  $dT/dt$  moving average  
 478 curve, hereafter  $A(dT/dt)$ , to measured  $\Delta^{17}\text{O}$  standard deviation ( $1\sigma$ ) (Figure A1). The  
 479 outlier in the trend is the direct result of an intentional disruption to the experimental run  
 480 (Experiment 5) in which the cooling fan intake on the TILDAS computer was blocked with  
 481 a sheet of paper for  $\sim 6$  minutes during the run.

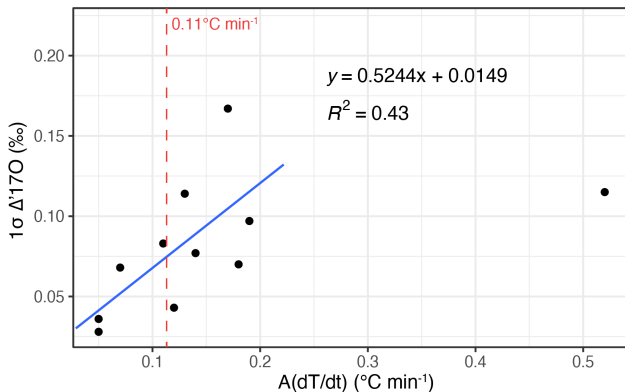


Figure 8: TILDAS electronics  $A(dT/dt)$  vs.  $1\sigma \Delta^{17}\text{O}$

482 For the system used in this project, it was realized that minimizing  $A(dT/dt)$  is the

483 most important factor in producing high-precision  $\Delta^{17}\text{O}$  measurements. To this end, it  
484 is best to perform analyses when there is no lab aircon control and the room is allowed  
485 to slowly heat up over the course of a measurement (Experiments 9 and 11). While the  
486 absolute temperature of the electronics typically increases by several degrees when applying  
487 this strategy, the continuous but consistent heating minimizes drastic instantaneous changes  
488 in  $dT/dt$  and therefore  $A(dT/dt)$ . Other, perhaps more practical long-term solutions to  
489 limit  $A(dT/dt)$  could be the extension of the liquid cooling system to include more sensitive  
490 electronic components, adding a heat exchanger near the computer's cooling fan intake, or  
491 using a high quality aircon with PID control to continuously supply the lab space around  
492 the TILDAS with air of consistent temperature.

493 In summary, the results of the experiments suggest the main control over measurement  
494 precision to be  $dT/dt$  of the TILDAS electronics. The internal purge rate and absolute  
495 temperature of the electronics had little to no influence on the measured  $\Delta^{17}\text{O}$  values, while  
496 the lab aircon temperature setting exerts its largest influence when set higher than the liquid  
497 chiller temperature. As the TILDAS system is constantly measuring and making corrections  
498 to adapt to its operational environment, it follows that rapid changes will exert a greater  
499 influence on instrument stability. Minimizing large instantaneous electronics temperature  
500 changes is key to achieving the necessary precision for relevant earth surface triple oxygen  
501 isotope studies using TILDAS.

## 502 **Experimental setup and details**

503 The first experiment began at 6:31am and lasted 66 minutes. Being the first analysis of  
504 the day the internal volume of the TILDAS instrument would have been equilibrated with  
505 bulk lab air both thermally and in its constituents. In an attempt to refresh the volume  
506 more quickly with dry  $\text{N}_2$ , the internal purge rate was set to approximately 1.5L/min. The  
507 observed positive trend in  $\Delta^{17}\text{O}$  values over the course of this run is assumed to be a result  
508 of the stabilizing of the instrument's internal environment.

Table 3: Summary of Results

Experiment	A(dT/dt) <sup>a</sup>	Avg. $\Delta^{17}\text{O}$	$1\sigma$ $\Delta^{17}\text{O}$
1	0.19	-0.061	0.097
2	0.18	0.036	0.070
3	0.14	-0.004	0.077
4	0.12	-0.005	0.043
5	0.52	-0.007	0.115
6	0.13	-0.043	0.114
7	0.07	0.026	0.068
8	0.11	-0.005	0.083
9	0.05	0.017	0.036
10	0.17	0.003	0.167
11	0.05	-0.031	0.082

<sup>a</sup> °C min<sup>-1</sup>

509 The second experiment started at 7:38am and lasted 60 minutes. During this run, the  
 510 internal purge rate was set at  $\sim 1\text{L}/\text{min}$  – the setting most commonly used for sample mea-  
 511 surements prior to, and since, these experiments. While measurement  $1\sigma$  precision improved  
 512 slightly to  $0.070\text{‰}$ , it is difficult to say whether the improvement was due to the different  
 513 purge rate or simply a result of a more stable measurement environment.

514 The third experiment started at 8:59am and lasted 38 minutes. This experiment again  
 515 tested the higher  $\text{N}_2$  purge rate of  $\sim 1.5\text{L}/\text{min}$ . The experiment resulted in a  $\Delta^{17}\text{O}$   $1\sigma$   
 516 precision of  $0.077\text{‰}$ , similar to the previous under a lower purge flow regime, with the  
 517 absolute  $\Delta^{17}\text{O}$  value,  $-0.004\text{‰}$ , being within error. This experiment lends support towards  
 518 the purge rate being a small factor in  $\Delta^{17}\text{O}$  precision.

519 The fourth experiment started at 10:02 and lasted 60 minutes. The parameters for this  
 520 experiment were setup identically to that of the second. The largest difference in operating  
 521 conditions between this experiment and each of the previous (and ultimately from all of the  
 522 following) experiments was simply the number of people in the instrument room. During  
 523 this experiment, 10 individuals spent notable amounts of time in the instrument room, as  
 524 compared to 1-3 for the previous runs. The high traffic during this run caused the room’s  
 525 aircon to activate more frequently. This is observed in the decreased A(dT/dt) (as a result  
 526 of less efficient cooling, i.e., decreased instantaneous cooling) and manifests in the nearly

527 halving of  $\Delta^{17}\text{O}$  standard deviation ( $1\sigma$ ) from the previous experiments to 0.043‰ with an  
528 average  $\Delta^{17}\text{O}$  of -0.005‰.

529 The fifth experiment started at 11:11am and lasted 45 minutes. This experiment is  
530 marked by the covering of the TILDS computer cooling fan intake for  $\sim 6$  minutes beginning  
531 at  $\sim 11:40$ am. The intent behind this action was to create an immediate, drastic change to  
532 the electronics environment to assess the impacts of temperature in real time. The resulting  
533  $dT/dt$  moving average curve from this action is a large double peak ( $A(dT/dt) = 0.52^\circ\text{C}$   
534  $\text{min}^{-1}$ ), the first of which is the rapid heating of the electronics when cooling air was cut off,  
535 and the second when the fan intake was uncovered, causing rapid cooling of the electronics.  
536 While the analysis resulted in good accuracy ( $\Delta^{17}\text{O} = -0.006‰$ ) this experiment resulted  
537 in an overall  $\Delta^{17}\text{O}$  ( $1\sigma$ ) of 0.115‰.

538 The sixth experiment started at 12:11am and lasted 57 minutes. This experiment was  
539 run under the higher  $\text{N}_2$  purge flow  $\sim 1.5\text{L}/\text{min}$ . Overall  $\Delta^{17}\text{O}$   $1\sigma$  precision was 0.114‰ and  
540 observably decreased throughout the run, correlated with inconsistent  $dT/dt$  peak frequency.  
541 There is no clear singular cause for this pattern.

542 The seventh experiment started at 13:31 and lasted 55 minutes. This experiment was  
543 run at the preferred  $\text{N}_2$  purge flow  $\sim 1\text{L}/\text{min}$ . For unclear reasons, electronics temperature  
544 stability was improved as evidenced by the decreased  $A(dT/dt)$  of  $0.07^\circ\text{C min}^{-1}$ . This  
545 marked the first experiment to achieve a  $A(dT/dt) < 0.1^\circ\text{C min}^{-1}$ . Despite this, the  $\Delta^{17}\text{O}$   
546  $1\sigma$  of 0.068‰ is not markedly improved relative to previous runs. The reason for this poorer  
547 than expected precision given the improved  $dT/dt$  profile is unclear.

548 The eighth experiment started at 14:34 and lasted 47 minutes. The experiment's setup  
549 was identical to the previous.  $A(dT/dt)$  of  $0.11^\circ\text{C min}^{-1}$  and  $\Delta^{17}\text{O}$   $1\sigma$  precision of 0.083‰  
550 are both expectedly similar to many of the previous experiments.

551 The ninth experiment started at 15:30 and lasted 45 minutes. The purge rate again was  
552 set to  $\sim 1\text{L}/\text{min}$ . This experiment is the first to test how the absence of aircon temperature  
553 control influenced measurement precision. The absolute temperature of the electronics in-



554 creased  $\sim 3^\circ\text{K}$ , roughly 3 times the temperature range observed in all previous experiments  
555 when lab aircon was in use. However,  $1\sigma$   $\Delta^{17}\text{O}$  precision was  $0.036\text{‰}$  and correlated to a  
556 low  $A(dT/dt)$  of  $0.05^\circ\text{C min}^{-1}$ , each of which are respectively the lowest of any experiment  
557 thus far. This experiment is a clear improvement in creating ideal measurement conditions  
558 and shows that absolute electronics temperature is not a major control on measurement  
559 precision.

560 The tenth experiment started at 16:39 and lasted 41 minutes. A  $\text{N}_2$  purge rate of  $\sim 1\text{L/min}$   
561 is maintained. This experiment tested setting lab aircon setpoint to  $24^\circ\text{C}$ , higher than the  
562 liquid chiller setpoint, to test the effects of potentially inconsistent cooling on the system.  
563 This experiment resulted in a high  $A(dT/dt)$  of  $0.17^\circ\text{C min}^{-1}$  and a correspondingly poor  
564  $\Delta^{17}\text{O}$   $1\sigma$  of  $0.167\text{‰}$  – by far the worst precision observed in this series of experiments. The  
565 electronics temperature profile is markedly different than previous experiments with aircon  
566 control, characterized by decreased regulation frequency and a larger absolute range.

567 The eleventh and final experiment started at 17:44 and lasted 52 minutes. Again a  
568  $\sim 1\text{L/min}$   $\text{N}_2$  purge rate is used. This experiment again tested the absence of lab aircon  
569 control on measurement precision, with similarly good results. Absolute electronics tem-  
570 perature increased  $\sim 3^\circ\text{K}$  with a similar profile to that of Experiment 9. The  $\Delta^{17}\text{O}$   $1\sigma$  of  
571  $0.028\text{‰}$  is the best achieved in any of the experiments performed. The low  $A(dT/dt)$  of  $0.05$   
572  $^\circ\text{C min}^{-1}$  matches that of experiment 9 in which lab aircon was also not used. While the  
573  $\Delta^{17}\text{O}$  value of  $-0.031\text{‰}$  is not within measurement error of the theoretical value of  $0.000\text{‰}$ ,  
574 the improvement of measurement precision is encouraging.

### 575 3. Labview code

576 All LabVIEW code, and TDLWintel ECL scripts can be found on github, here:

577 <https://github.com/vinhare/UCT-TILDAS-17O>

578 Please cite as:DOI :10.5281/zenodo.6802227

579 **AutoCart LabVIEW valves, volumes, and sample sequences**

580 **Mixing volumes**

581 Mixing volume 1 (MV1) – 586mL (flask + V16-V17 volume)

582 Mixing volume 2 (MV2) – 61mL (liquid N<sub>2</sub> trap)

583 Mixing volume 3 (MV3) – 40mL (bellows)

584 **AutoCart valves**

585 V1 (diaphragm valve) – Up-stream end of cracker 1

586 V2 (diaphragm valve) – Up-stream end of cracker 2

587 V3 (diaphragm valve) – Up-stream end of cracker 3

588 V4 (diaphragm valve) – Down-stream end of cracker 1

589 V5 (diaphragm valve) – Down-stream end of cracker 2

590 V6 (diaphragm valve) – Down-stream end of cracker 3

591 V7 (diaphragm valve) – Inlet for N<sub>2</sub> supply

592 V8 (3-way solenoid valve) – N<sub>2</sub> supply director (normally open to break-seal manifold, nor-  
593 mally closed to V21/MV3)

594 V16 (diaphragm valve) – Separates sample inlet side from preparation side of AutoCart

595 V17 (diaphragm valve) – Separates flask volume from liquid N<sub>2</sub> trap

596 V18 (diaphragm valve) – Separates liquid N<sub>2</sub> trap from MV3

597 V19 (diaphragm valve) – Inlet from AutoCart to TILDAS switching valve system

598 V20 (diaphragm valve) – To vacuum pump

599 V21 (diaphragm valve) – Dilution N<sub>2</sub> shut-off

600 Circulation Loop (2x diaphragm valve) – 2 pneumatically connected valves at either end of  
601 the circulation loop

602 Manual toggle valve separating GasBench system & AutoCart

603 Manual twist valve separating cracker manifold & AutoCart

604

605 **Carbonate samples from GasBench**

- 606 • Reset all sample data values to 0
- 607 • Open V7
- 608 • Open V16
- 609 • User input – close off flask via stopcocks
- 610 • Open circulation loop and pump out for 60 seconds
- 611 • Open V8 – Switch N<sub>2</sub> direction to V21/MV3
- 612 • Close V20
- 613 • Open V21
- 614 • Pressurize circulation loop to 1300 mbar
- 615 • Close V21
- 616 • Briefly (1-2 seconds) circulate dry N<sub>2</sub> through loop via diaphragm pump
- 617 • Close circulation loop
- 618 • Close V8 – Switch N<sub>2</sub> direction away from V21/MV3
- 619 • Open V20 – pump system down to <76 mtorr
- 620 • Close manual valve connecting AutoCart to cracker manifold
- 621 • Open manual valve connecting GasBench system to AutoCart
- 622 • Pump out GasBench capillary for 30 seconds
- 623 • Raise liquid N<sub>2</sub> dewar and allow liquid N<sub>2</sub> trap to cool
- 624 • Manually restrict flow from vacuum pump to AutoCart via twist valve
- 625 • Use GasBench sampling needle to direct sample gas through the GasBench and to the
- 626 AutoCart
- 627 • 40-minute sample transfer wait time
- 628 • Direct GasBench system away from AutoCart
- 629 • Pump AutoCart to <75 mtorr
- 630 • Close V16
- 631 • Close V17
- 632 • Close V18

- 633 • Close manual valve connecting GasBench system to AutoCart
- 634 • Remove liquid N<sub>2</sub> dewar from trap
- 635 • Allow 6 minutes for sample to thaw
- 636 • Read thaw pressure and calculate  $\mu\text{mol CO}_2$  trapped and dilution requirements
- 637 • Open left flask stopcock to allow sample into flask (MV1)
- 638 • Open V17 – expand sample into flask 40 seconds
- 639 • Close V17
- 640 • Close V20
- 641 • Open V8 – Switch N<sub>2</sub> direction towards V21/MV3
- 642 • Open V21 – build N<sub>2</sub> pressure in MV3 for 30 seconds
- 643 • Open V18
- 644 • Begin turbulent mixing steps – repeat n times as determined by measured CO<sub>2</sub> yield
  - 645 o Pressurize MV3 + MV2 to 1450 mbar
  - 646 o Open V17
  - 647 o 5 second expansion into MV1
  - 648 o Close V17
- 649 • If turbulent mixing steps don't achieve required P, N<sub>2</sub> is added non-turbulently until nec-  
650 essary pressure (Dilution Target Pressure) is reached
- 651 • Close V17
- 652 • Close V8 – Switch N<sub>2</sub> direction away from V21/MV3
- 653 • Close V21
- 654 • Open V20
- 655 • Pump out leftover N<sub>2</sub> from MV3 + MV2 for 2 minutes
- 656 • Close V20
- 657 • Open V17 – expand diluted sample from MV1 through MV2 + MV3
- 658 • Measure sample final pressure
- 659 • Open V16

660 • Open circulation loop valves turn on diaphragm pump for 150 seconds

661 • Close circulation loop valves turn off diaphragm pump

662 • Close V16

663 • Open V19 and begin TILDAS analysis

664

665 **Break-seal samples from AutoCart mount**

666 Written for samples from break-seal 1 (2) (3)

667

668 • Reset all sample data values to 0

669 • Open V7

670 • Open V16

671 • Close V5 (4) (4)

672 • Close V6 (6) (5)

673 • User input – close off flask via stopcocks

674 • Close both manual valves connecting AutoCart to cracker manifold and GasBench

675 • Open circulation loop and pump out for 60 seconds

676 • Open V8 – Switch N<sub>2</sub> direction towards V21/MV3

677 • Close V20

678 • Open V21

679 • Pressurize circulation loop to 1300 mbar

680 • Close V21

681 • Briefly (1-2 seconds) circulate dry N<sub>2</sub> through loop via diaphragm pump

682 • Close circulation loop

683 • Close V8 – Switch N<sub>2</sub> direction away from V21/MV3

684 • Open V20

685 • Open manual valve connecting cracker manifold to AutoCart

686 • Open V4 (5) (6)

- 687 • Pump system down to <76 mtorr
- 688 • Raise liquid N<sub>2</sub> dewar and allow liquid N<sub>2</sub> trap to cool
- 689 • Close V18
- 690 • Break break-seal containing sample
- 691 • Allow 10 minutes for cryo-pull trapping of sample CO<sub>2</sub>
- 692 • Open V18
- 693 • Pump over frozen sample to <75 mtorr
- 694 • Close V17
- 695 • Close V18
- 696 • Close V16
- 697 • Close V4 (5) (6)
- 698 • Remove liquid N<sub>2</sub> dewar from trap
- 699 • Allow 6 minutes for sample to thaw
- 700 • Close manual valve connecting AutoCart to cracker manifold
- 701 • Open left flask stopcock to allow sample into flask (MV1)
- 702 • Read thaw pressure and calculate  $\mu\text{mol CO}_2$  trapped and dilution requirements
- 703 • Open V17 – expand sample into MV1 for 40 seconds
- 704 • Close V17
- 705 • Close V20
- 706 • Open V8 – Switch N<sub>2</sub> direction towards V21/MV3
- 707 • Open V21 – build N<sub>2</sub> pressure in MV3 volume for 30 seconds
- 708 • Open V18
- 709 • Begin turbulent mixing steps – repeat n times as determined by measured CO<sub>2</sub> yield
  - 710 o Pressurize MV3 + MV2 to 1450 mbar
  - 711 o Open V17
  - 712 o 5 second expansion into MV1
  - 713 o Close V17

- 714 • If turbulent mixing steps don't achieve required P, N<sub>2</sub> is added non-turbulently until nec-
- 715 essary pressure (Dilution Target Pressure) is reached
- 716 • Close V17
- 717 • Close V8 – Switch N<sub>2</sub> direction away from V21/MV3
- 718 • Close V21
- 719 • Open V20
- 720 • Pump out leftover N<sub>2</sub> from MV3 + MV2 for 2 minutes
- 721 • Close V20
- 722 • Open V17 – expand diluted sample from MV1 through MV2 + MV3
- 723 • Measure sample final pressure
- 724 • Open V16
- 725 • Open circulation loop valves turn on diaphragm pump for 150 seconds
- 726 • Close circulation loop valves turn off diaphragm pump
- 727 • Close V16
- 728 • Open V19 and begin TILDAS analysis
- 729     **Atmospheric flask samples**
- 730 • Start assuming flask has been replaced inline on AutoCart and headspace evacuated
- 731 • Reset all sample data values to 0
- 732 • Open V7
- 733 • Open V16
- 734 • Close manual valve connecting cracker manifold to AutoCart
- 735 • Close manual valve connecting GasBench system to AutoCart
- 736 • Open circulation loop and pump out for 60 seconds
- 737 • Open V8 – Switch N<sub>2</sub> direction to V21/MV3
- 738 • Close V20
- 739 • Open V21
- 740 • Pressurize circulation loop to 1300 mbar

- 741 • Close V21
- 742 • Briefly (1-2 seconds) circulate dry N<sub>2</sub> through loop via diaphragm pump
- 743 • Close circulation loop
- 744 • Close V8 – Switch N<sub>2</sub> direction away from V21/MV3
- 745 • Open V20 – pump system down to <76 mtorr
- 746 • Close V16
- 747 • Close V17
- 748 • Open flask stopcocks to open sample to V16-17 volume (MV1)
- 749 • Raise liquid N<sub>2</sub> dewar and allow liquid N<sub>2</sub> trap to cool
- 750 • Manually restrict flow from vacuum pump to AutoCart via twist valve
- 751 • Open V17
- 752 • Pump flask through liquid N<sub>2</sub> trap to < 90 mtorr
- 753 • Close V17
- 754 • Close V18
- 755 • Remove liquid N<sub>2</sub> dewar from trap
- 756 • Allow 6 minutes for sample to thaw
- 757 • Read thaw pressure and calculate  $\mu\text{mol CO}_2$  trapped and dilution requirements
- 758 • Open left flask stopcock to allow sample into flask (MV1)
- 759 • Open V17 – expand sample into flask 40 seconds
- 760 • Close V17
- 761 • Close V20
- 762 • Open V8 – Switch N<sub>2</sub> direction towards V21/MV3
- 763 • Open V21 – build N<sub>2</sub> pressure in MV3 volume for 30 seconds
- 764 • Open V18
- 765 • Begin turbulent mixing steps – repeat n times as determined by measured CO<sub>2</sub> yield
  - 766     o Pressurize MV3 + MV2 to 1450 mbar
  - 767     o Open V17



- 768       o 5 second expansion into MV1
- 769       o Close V17
- 770   • If turbulent mixing steps don't achieve required P, N<sub>2</sub> is added non-turbulently until
- 771 necessary pressure (Dilution Target Pressure) is reached
- 772   • Close V17
- 773   • Close V8 – Switch N<sub>2</sub> direction away from V21/MV3
- 774   • Close V21
- 775   • Open V20
- 776   • Pump out leftover N<sub>2</sub> from MV3 + MV2 for 2 minutes
- 777   • Close V20
- 778   • Open V17 – expand diluted sample from MV1 through MV2 + MV3
- 779   • Measure sample final pressure
- 780   • Open V16
- 781   • Open circulation loop valves turn on diaphragm pump for 150 seconds
- 782   • Close circulation loop valves turn off diaphragm pump
- 783   • Close V16
- 784   • Open V19 and begin TILDAS analysis

## 785 **Sequence summary**

786 Each of the 3 sequence types handled by the LabVIEW code can be summarized by being  
787 split into three parts. For each of them, the first part is preparation of the circulation loop  
788 later used for mixing the diluted sample gas, the second part cryo-trapping and pumping  
789 over of the sample gas, and the third part, which is identical for all sequences and sample  
790 types, is the thawing, diluting, and mixing of the sample gas. Following is a summary of  
791 the sample preparation sequences currently incorporated in the LabVIEW code. Information  
792 regarding valve type, mixing volumes, and step by step breakdowns for each of the sequences  
793 can be found in the supplementary file "AutoCart LabVIEW valves, volumes, and sample

794 sequences".

795       Preparing the circulation loop happens identically for all sample sequences. First, the  
796 loop is manually evacuated then filled with high purity N<sub>2</sub> to 1100 mbar. The sequence is  
797 then started, the first steps being the re-evacuation of the loop and subsequent pressurizing to  
798 1300 mbar of the same high-purity N<sub>2</sub>. The inline diaphragm pump is then briefly activated  
799 to cycle gas through the loop, moving any potential atmosphere leak during evacuation into a  
800 more easily evacuated volume and recharging the loop with N<sub>2</sub>. The circulation loop is then  
801 closed off on either end and allowed to slowly leak N<sub>2</sub> during the duration of the respective  
802 sample preparation sequences.

803       The preparation sequences differ in the sample transfer, cryo-trapping, and post-trapping  
804 cleaning steps. Carbonate samples introduced via the GasBench II are manually sampled  
805 via the sampling needle and directed into the AutoCart upstream of MV1. The CO<sub>2</sub> passes  
806 over the flask via a bypass as the flask valves are closed at this point and is cryo-trapped in  
807 MV2. A transit time of 40 minutes is allotted for comprehensive transfer and collection of  
808 sample CO<sub>2</sub> from the sampling vials. MV2 is the vacuum pumped over the frozen sample  
809 gas to 75 mTorr before sample thaw.

810       Samples introduced via break-seals on the cracker manifold are cryo-pulled under static  
811 vacuum into MV2 for 10 minutes, passing over the flask via the same bypass. After 10  
812 minutes, the full volume is vacuum pumped over the frozen sample gas to 75 mTorr before  
813 sample thaw.

814       Atmospheric samples introduced by connecting the sampling flask to the AutoCart as  
815 MV1 are handled initially by evacuating the MV1 head-space created. Once evacuated, MV1  
816 is closed off at valves 16 and 17 and the flask valves opened. The sample is then restrictively  
817 vacuum pumped through the cryo-trap on MV2 to 90 mTorr. Once achieved, the sample is  
818 thawed in MV2. This process typically takes ~50 minutes. It is of suspicion that a small  
819 amount of atmospheric N<sub>2</sub> condenses in the cryo-trap during this process. This excess gas is  
820 accounted for by a small offset in the sample yield when calculating dilution specifications.

821 For all sequences samples are allowed to thaw for 6 minutes in MV2 before the yield is  
822 measured. Measured yields are then used to calculate sample dilution requirements including  
823 amount of N<sub>2</sub> to be added and the number of turbulent mixing steps to be performed. The  
824 sample CO<sub>2</sub> is expanded into MV1 and signifies the beginning of the dilution and mixing  
825 process.

826 Sample dilution and initial mixing takes place in MV1 and is done by repeatedly pressur-  
827 izing MV3 and MV2 to 1450 mbar of N<sub>2</sub> and subsequently expanding into MV1. The large  
828 pressure change combined with the flask's specific design to maximize turbulence promote  
829 even sample dilution. After pressure equilibration, MV1 is isolated and MV3 and MV2 re-  
830 pressurized to 1450 mbar. These steps are repeated  $n$  times as determined by measured sam-  
831 ple yield (typically 4-5).  $n$  is calculated according to the curve  $n = 3e^{-6}x^2 + 0.0031x + 0.0261$ ,  
832 where  $x$  is the target dilution pressure.  $n$  need not strictly be rounded to a whole number  
833 but can be a decimal under the condition that the fraction of  $n$  multiplied by 1450 mbar  
834 is greater than the pressure already contained in MV1 after the previous expansion. For  
835 example, when  $n = 4.872$ ,  $0.872 \times 1450 \text{ mbar} = 1264.4 \text{ mbar}$ . Typical MV1 pressure af-  
836 ter 4 expansions is  $\sim 765 \text{ mbar}$ , so an expansion of 1264.4 mbar would occur to complete  
837 sample dilution. In the event that a partial expansion cannot occur (e.g. when  $n = 4.123$ ,  
838  $0.123 \times 1450 \text{ mbar} = 178.4 \text{ mbar}$ , less than MV1 pressure),  $n$  is rounded down to the near-  
839 est whole number and N<sub>2</sub> is then non-turbulently added to MV1 via valve V21 until the  
840 calculated dilution pressure is reached.

841 The direction of N<sub>2</sub> flow from MV3 through MV2 and into MV1, combined with the  
842 earlier expansion of the sample CO<sub>2</sub>, concentrates the sample in MV1. This causes an excess  
843 of N<sub>2</sub> in MV2 and MV3 at the end of the dilution process. To overcome this, dilution  
844 requirements are calculated with respect to MV1 (586mL) rather than the combined volume  
845 of MV1,2,3 (687 mL). After the dilution process is complete, V17 closes, isolating MV1,  
846 and MV2 and MV3 are evacuated. MV1 is then expanded to MV1,2,3, thereby achieving  
847 accurate sample dilution throughout the entirety of the mixing volumes where true dilution

848 pressure and accuracy are recorded.

849 Further mixing occurs as the circulation loop is opened to the full mixing volume and the  
850 diaphragm pump activated. The diaphragm pump circulates at 750mL/min for 2.5 minutes,  
851 allowing sample gas to circulate through the entirety of the cart ~3 times. After 2.5 minutes  
852 of circulating the diaphragm pump is switched off, the loop is closed, and sample preparation  
853 is considered complete.

854 **4.  $\delta^{13}\text{C}$  data**

Table 4:  $\delta^{13}\text{C}$  data for  $\text{CO}_2$  evolved by phosphoric acid digestion of interlaboratory carbonate standards at  $70^\circ\text{C}$ , measured by TILDAS.  $\delta^{13}\text{C}_{\text{meas}}$  values for individual aliquots are corrected to VPDB using the IAEA603 ( $\text{CaCO}_3$ ) and NBS18 ( $\text{CaCO}_3$ ) values recommended by the IAEA (<https://nucleus.iaea.org/sites/ReferenceMaterials/Pages/Stable-Isotopes.aspx>). See Table 1 for corresponding oxygen isotope data. Fitted coefficients (eq. 3, main text) are  $A_{636} = 42$ ,  $b_{636} = -340$ ,  $b_{626} = 1.03$

Sample	$\delta^{13}\text{C}$	$\delta^{13}\text{C}_{\text{corr}}^a$
IAEA603-4	43.13	2.39
IAEA603-5	43.24	2.47
IAEA603-6	43.33	2.54
IAEA603-7	43.15	2.41
IAEA603-9	43.30	2.51
IAEA603-10	43.14	2.34
<b>Average</b>	<b>43.21</b>	<b>2.44</b>
$\pm 1\sigma$	<b>0.09</b>	<b>0.08</b>
<b>St. err<sup>b</sup></b>	<b>0.04</b>	<b>0.03</b>
NBS18-8	35.76	-4.78
NBS18-12	35.75	-4.82
NBS18-13	35.22	-5.32
NBS18-14	35.56	-5.00
<b>Average</b>	<b>35.57</b>	<b>-4.98</b>
$\pm 1\sigma$	<b>0.25</b>	<b>0.25</b>
<b>St. err<sup>b</sup></b>	<b>0.13</b>	<b>0.12</b>
NBS19-5	42.56	1.82
NBS19-6	42.68	1.96
NBS19-7	42.76	1.99
NBS19-11	42.67	1.89
NBS19-12	42.57	1.82
NBS19-13	42.60	1.84
NBS19-14	42.60	1.86
<b>Average</b>	<b>42.63</b>	<b>1.88</b>
$\pm 1\sigma$	<b>0.07</b>	<b>0.07</b>
<b>St. err<sup>b</sup></b>	<b>0.03</b>	<b>0.03</b>

<sup>a</sup> Corrected using eq. (3), but for  $\delta^{13}\text{C}$ ; <sup>b</sup> Standard error =  $1\sigma/\sqrt{n}$